distributions of the position histograms as a function of GSO pixel position for horizontal and vertical directions are shown in Fig. 5(A) and (B), respectively. The P/V distributions in horizontal direction were the average of the 15 profiles while those in vertical direction were the average of 20 profiles. The P/Vs of the both edges for vertical direction did not analyze because we could not obtain the enough peak counts. We evaluated the P/Vs for upper, lower layers and without pulse shape discrimination.

3.1.2. Energy resolution

We show energy spectra for the upper layer (GSO with 1.5 mol% Ce), lower layer (GSO with 0.4 mol% Ce) and without pulse-shape discrimination, in Fig. 6(A), (B) and (C), respectively. The average energy resolutions of the upper layer, lower layer and without pulse-shape discrimination were $28.0 \pm 3.6\%$ full-width at half-maximum (FWHM), $26.2 \pm 3.0\%$ FWHM and $28.4 \pm 3.1\%$ FWHM, respectively. The energy resolutions as a function of horizontal and vertical GSO pixel position for each layer and without pulse-shape discrimination are shown in Fig. 7(A) and (B), respectively. In addition, we showed the energy peak channel numbers as a function of horizontal and vertical GSO pixel position in Fig. 8(A) and (B), respectively.

3.1.3. Pulse-shape spectra

The pulse-shape spectra of the GSO DOI block detector are shown in Fig. 9. The right peak corresponds to the upper layer (1.5 mol% Ce) and the left peak corresponds to the lower layer (0.4 mol% Ce). The pulse shape spectra showed good separation with an average P/V of 5.2 ± 1.7. The P/Vs of the pulse shape spectra as a function of the horizontal and vertical GSO pixel positions in Fig. 10(A) and (B), respectively.

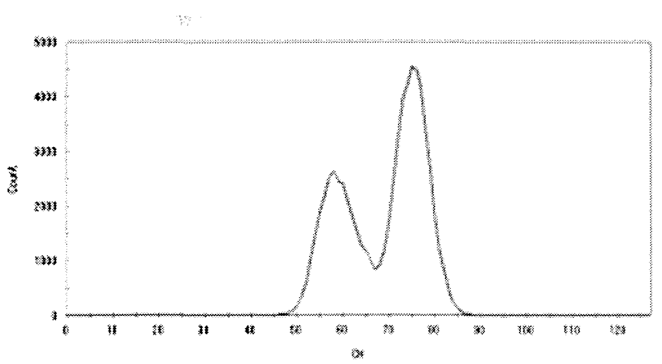

Fig. 9. Pulse-shape spectra of GSO DOI block detector.

4. Discussion

We could successfully develop dual-layer GSO DOI block detectors arranged in two GSO scintillator blocks on one PSPMT with two angled optical fiber-based image guides. With the developed block detectors, we could arrange the GSO blocks in a nearly circular shape with eight PSPMTs.

The developed phoswich DOI block detectors discriminate the DOI using pulse-shape analysis. For this purpose, scintillators with similar light outputs and different decay times are required. GSOs are a good choice because GSO decay time can be changed with the amount of the Ce concentrations. We used two types of GSO with 1.5 mol% Ce with decay time of 39 ns, and 0.4 mol% Ce with decay time of 63 ns. These decay time differences were sufficient to distinguish DOI detection by pulse-shape analysis.

We could clearly resolve almost all pixels in the block detector (Fig. 4(A)–(C)). In these, Fig. 4(A) (1.5 mol% Ce: upper layer) showed better separation in the two-dimensional histograms than Fig. 4(B) (0.4 mol% Ce: lower layer). The P/Vs distributions shown in Fig. 5 for the upper layer in horizontal and vertical directions were also better than the lower layer. This is because the lower layer contained the inter-crystal scattered events both from upper layer and lower layer. The probability of forward Compton scattered (small angled) events is higher than the back scattered events for 662-keV gamma photons. Therefore, the upper layer contained fewer inter-crystal scattered events.

We used optical fiber-based image guides to arrange the two scintillator blocks at 22.5°. The distortions had seldom been observed in the two-dimensional histograms of the GSO block detector (Fig.4(A)–(C)) because the optical fiber-based image guides preserved the distribution of the scintillation light. Therefore, the optical fiber-based image guides are suitable for the development of these types of angled block detectors.

The energy spectra of the upper layer (Fig. 6(A)) shows higher scatter components than those of the lower layer (Fig. 6(B)). One of the explanations of this phenomenon is that the upper layer absorbed more scattered gamma photons from the Cs-137 gamma photons than the lower layer. Furthermore, the lower layer detected lower scattered photons than the upper layer.

5. Conclusion

We developed dual-layer GSO DOI block detectors using angled optical fiber-based image guides. Almost a circular ring could be realized with the 8 developed block detectors. The developed block detectors are promising for small-ring-diameter high resolution and high-sensitivity PET systems.

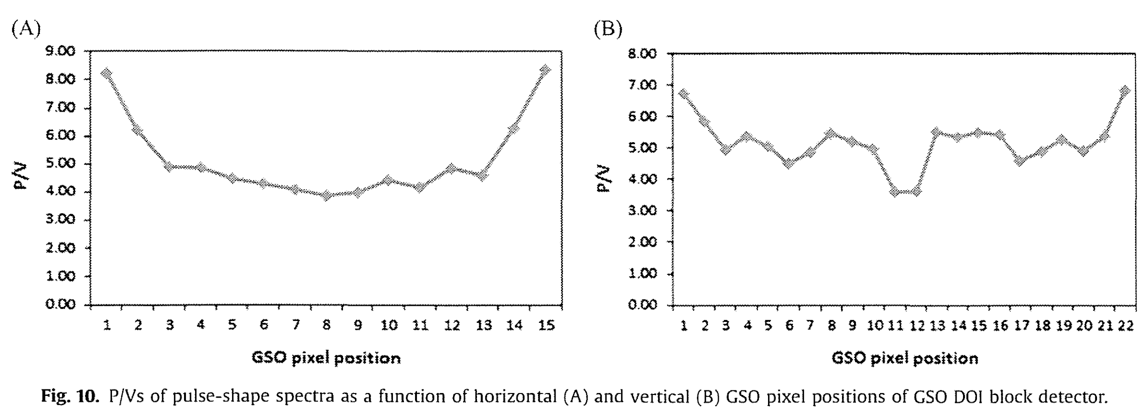

Fig. 10. P/Vs of pulse-shape spectra as a function of horizontal (A) and vertical (B) GSO pixel positions of GSO DOI block detector.

References

[1] W.W. Moses, S.E. Derenzo, IEEE Transactions Nuclear Science NS41 (1994) 1441.

[2] A. Del Guerra, G. Di Domenico, M. Scandola, G. Zavattini, Nuclear Instruments and Methods in Physics Research Section A 409 (1998) 537.

[3] S.R. Cherry, Y. Shao, R.W. Silverman, K. Meadors, S. Siegel, A. Chatziioannou, J.W. Young, W.F. Jones, J.C. Moyers, D. Newport, A. Boutefnouchet, T.H. Farquhar, M. Andreaco, M.J. Paulus, D.M. Binkley, R. Nutt, M.E. Phelps, IEEE Transactions on Nuclear Science NS44 (1997) 1161.

[4] Y-C. Tai, A.F. Chatziioannou, Y. Yang, R.W. Silverman, K. Meadors, S. Siegel, D. F. Newport, J.R. Stickel, S.R. Cherry, Physics in Medicine and Biology 48 (2003) 1519.

[5] H. Wu, D. Pal, T.Y. Song, J.A. O'Sullivan, Y-C. Tai, Journal of Nuclear Medicine 49 (2008) 1668.

[6] C-M. Kao, Q. Xie, Y. Dong, L. Wan, C-T. Chen, IEEE Transactions on Nuclear Science NS56 (6) (2009) 2678.

[7] R.S. Miyaoka, M.L. Janes, K. Lee, B. Park, P.E. Kinahan, T.K. Lewellen, Molecular Imaging 4 (2005) 117.

[8] S.I. Ziegler, B.J. Pichler, G. Boening, M. Rafecas, W. Pimpl, E. Lorenz, N. Schmitz, M. Schwaiger, European Journal of Nuclear Medicine 28 (2001) 136.

[9] R. Boellaard, F. Buijs, H.W.A.M. de Jong, M. Lenox, T. Gremillion, A.A. Lammertsma, Physics in Medicine and Biology 48 (2003) 429.

[10] F. Sánchez, L. Moliner, C. Correcher, A. González, A. Orero, M. Carles, A. Soriano, M.J. Rodriguez-Alvarez, L.A. Medina, F. Mora, J.M. Benlloch, Medical Physics 39 (2) (2012) 643.

[11] S.I. Kwon, J.S. Lee, H.S. Yoon, M. Ito, G.B. Ko, J.Y. Choi, S-H. Lee, I.C. Song, J.M. Jeong, D.S. Lee, S.J. Hong, Journal of Nuclear Medicine 52, 572.

[12] Y-C. Tai, A. Ruangma, D. Rowland, S. Siegel, D.F. Newport, P.L. Chow, R. Laforest, Journal of Nuclear Medicine 46 (2005) 455.

[13] Y.C. Tai, A. Chatziioannou, S. Siegel, J. Young, D. Newport, R.N. Goble, R.E. Nutt, S.R. Cherry, Physics in Medicine and Biology 46 (2001) 1845.

[14] S. Surti, J.S. Karp, A.E. Perkins, C.A. Cardi, M.E. Daube-Witherspoon, A. Kuhn, G. Muehllehner, IEEE Transactions on Medical Imaging 24 (2005) 844.

[15] T. Yamaya, E. Yoshida, T. Inaniwa, S. Sato, Y. Nakajima, H. Wakizaka, D. Kokuryo, A. Tsuji, T. Mitsuhashi, H. Kawai, H. Tashima, F. Nishikido, N. Inadama, H. Murayama, H. Haneishi, M. Suga, S. Kinouchi, Physics in Medicine and Biology 56 (2011) 1123.

[16] C. Knoess, S. Siegel, A. Smith, D. Newport, N. Richerzhagen, A. Winkeler, A. Jacobs, R. N. Goble, R. Graf, K. Wienhard, W-D. Heiss, European Journal of Nuclear Medicine and Molecular Imaging 30 (2003) 737.

[17] J.A. Correia, C.A. Burnham, D. Kaufman, A-L. Brownell, A.J. Fischman, IEEE Transactions on Nuclear Science NS51 (1) (2004) 21.

[18] A.F. Chatziioannou, S.R. Cherry, Y. Shao, R.W. Silverman, K. Meadors, T. H. Farquhar, M. Pedarsani, M.E. Phelps, Journal of Nuclear Medicine 40 (7) (1999) 1164.

[19] S. Ahn, S.M. Kim, J. Son, D.S. Lee, J.S. Lee, Medical Physics 39 (2012) 589.

[20] H.W. de Jong, F.H. van Velden, R.W. Kloet, F.L. Buijs, R. Boellaard, A.A. Lammertsma, Physics in Medicine and Biology 52 (2007) 1505.

[21] S. Yamamoto, H. Watabe, Y. Kanai, T. Watabe, K. Kato, J. Hatazawa, Physics in Medicine and Biology 58 (2013) 7875.

[22] S. Yamamoto, M. Imaizumi, T. Watabe, H. Watabe, Y. Kanai, E. Shimosegawa, J. Hatazawa, Physics in Medicine and Biology 55 (2010) 5817.

[23] S. Yamamoto, M. Imaizumi, Y. Kanai, M. Tatsumi, M. Aoki, E. Sugiyama, M. Kawakami, E. Shimosegawa, J. Hatazawa, Annals of Nuclear Medicine 24 (2010) 89.

[24] S. Yamamoto, Nuclear Instruments and Methods in Physics Research Section A 587 (2008) 319.